NANO LETTERS

Letter

pubs.acs.org/NanoLett

# Combinatorial Discovery of Lanthanide-Doped Nanocrystals with Spectrally Pure Upconverted Emission

Emory M. Chan,* Gang Han,‡ Joshua D. Goldberg, Daniel J. Gargas, Alexis D. Ostrowski, P. James Schuck, Bruce E. Cohen, and Delia J. Milliron*

The Molecular Foundry, Lawrence Berkeley National Laboratory, Berkeley, California 94720, United States

Supporting Information

**ABSTRACT:** Nanoparticles doped with lanthanide ions exhibit stable and visible luminescence under near-infrared excitation via a process known as upconversion, enabling long-duration, low-background biological imaging. However, the complex, overlapping emission spectra of lanthanide ions can hinder the quantitative imaging of samples labeled with multiple upconverting probes. Here, we use combinatorial screening of multiply doped $NaYF_4$ nanocrystals to identify a series of doubly and triply doped upconverting nanoparticles that exhibit narrow, spectrally pure emission spectra at various visible wavelengths. We then developed a comprehensive kinetic model validated by our extensive experimental data set. Applying this model, we elucidated the energy transfer mechanisms giving rise to spectrally pure emission. These mechanisms suggest design rules for electronic level structures that yield robust color tuning in lanthanide-doped upconverting nanoparticles. The resulting materials will be useful for background-free multicolor imaging and tracking of biological processes.

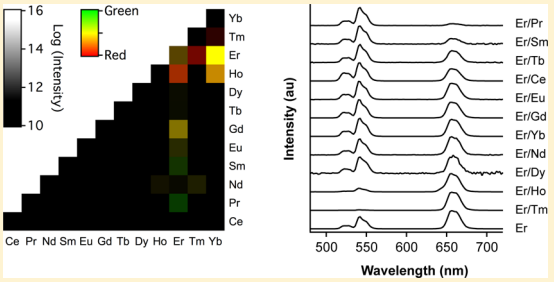


**KEYWORDS:** *Phosphors, luminescence, high-throughput, energy transfer, near-infrared, screening*

Colloidal nanoparticles doped with combinations of lanthanide ions[1,2] such as $Yb^{3+}$ and $Er^{3+}$ have emerged as promising optical probes for biological imaging[3,4] and single-molecule tracking.[4−6] These materials, when excited with near-infrared (NIR) radiation, emit exceptionally stable[5,7] and visible luminescence,[8,9] a process termed upconversion, making the nanoparticles ideal for extended imaging of cells and internal organs.[10] However, the abundance of $4f^N$ electronic states[11] in lanthanide ions typically leads to multiple overlapping emission lines,[12] thereby precluding the simultaneous tracking and quantitation of large numbers of colocalized species.

To overcome this challenge, we used energy transfer to selectively populate specific energy states of lanthanide emitters by incorporating different lanthanide ions in a single nanocrystal, thus facilitating the alignment of targeted donor and acceptor transitions—an approach that has been largely unexplored. In this work, we show how combinatorial screening[13,14] and high-throughput methods[15] can be used to uncover upconverting nanoparticles (UCNPs) with dopant compositions that are ideally suited for either pure green or pure red emission. A theoretical model validated by these observations was developed and used to deduce the selective population mechanisms underlying this spectrally pure emission and to derive general design principles for alignment of dopant energy levels and therefore the fine-tuning of optical properties.

Earlier reports of color tuning in upconverting materials[1] typically have relied on the crude blending of multiple emission peaks.[16−18] Efforts to achieve spectrally pure, single-color emission have been limited to quenching undesired transitions by employing either ligands with high-energy vibrational modes[19] or inorganic host matrices with high phonon energies,[20,21] both of which sacrifice the intensity of desired transitions, as well. A more promising approach involves energy transfer between coupled lanthanide dopants[22−24] or between lanthanide ions and transition metals.[25,26] However, the very complexity of electronic structure[11] that provides opportunities for advantageous energy transfer also makes it difficult to pinpoint the effective lanthanide ion combinations among the vast number of possibilities. Mapping the composition space using high-throughput methods, as we have done in this report, is the key to circumventing all of these limitations.

**Binary Doping.** To identify promising energy transfer interactions between lanthanide ions, we initially synthesized $NaYF_4$ nanocrystals[27] doped with the 78 binary and unary combinations of 12 different lanthanide ions ($Ce^{3+}$, $Pr^{3+}$, $Nd^{3+}$, $Sm^{3+}$, $Eu^{3+}$, $Gd^{3+}$, $Tb^{3+}$, $Dy^{3+}$, $Ho^{3+}$, $Er^{3+}$, $Tm^{3+}$, and $Yb^{3+}$). To accomplish this, we utilized an automated nanocrystal synthesis robot[28] to prepare 500 $\mu$L-scale reactions of trifluoroacetate precursors[28−30] in 96-well plates (see Supporting Information for additional experimental details). Each lanthanide species was substitutionally doped at 2 mol %, e.g. $NaYF_4$:2% $Er^{3+}$ is $NaY_{0.98}Er_{0.02}F_4$. Employing the common excitation wavelength of 980 nm (10 W/cm$^2$, continuous-wave) in a custom

**Received:** May 12, 2012
**Revised:** June 11, 2012





dx.doi.org/10.1021/nl3017994 | *Nano Lett.* XXXX, XXX, XXX−XXX

microplate reader, we observed visible upconverted luminescence (UCL) only in nanocrystals containing $Er^{3+}$ or $Yb^{3+}$ ions (Figure 1a), which are the only lanthanides with appreciable absorption cross sections around 980 nm.[11,12]

While $Yb^{3+}$-sensitized materials are well-known in bulk and nanoscale materials as being the most efficient upconverters, in our screen they either did not exhibit high spectral purity or did not exhibit high intensity emission in the visible spectrum. Therefore, we focused our investigation on the less-studied $Er^{3+}$-doped upconverting nanoparticles (UCNPs), because $Er^{3+}$-doped UCNPs codoped with $Tm^{3+}$ or $Ho^{3+}$ exhibited preferential red emission, while $Er^{3+}/Sm^{3+}$ and $Er^{3+}/Pr^{3+}$ exhibited preferential green emission (Figure 1a). The luminescence spectra of $Er^{3+}$-containing, codoped UCNPs (Figure 1b) exhibited green (525, 540 nm) and red (660 nm) peaks corresponding to the $Er^{3+}$ $^2H_{11/2}/^4S_{3/2}\rightarrow{}^4I_{15/2}$ and $^4F_{9/2}\rightarrow{}^4I_{15/2}$ transitions, respectively, as unambiguously identified in the spectrum of the singly doped $NaYF_4$:2% $Er^{3+}$ UCNPs. This indicates that $Er^{3+}$ is acting as both the absorber and emitter in all these nanoparticles. Nonetheless, the presence of codopants modulates the relative red and green emission peak intensities. We attribute this modulation to a series of energy transfer processes between $Er^{3+}$ and the codopant, as elucidated in a following section.

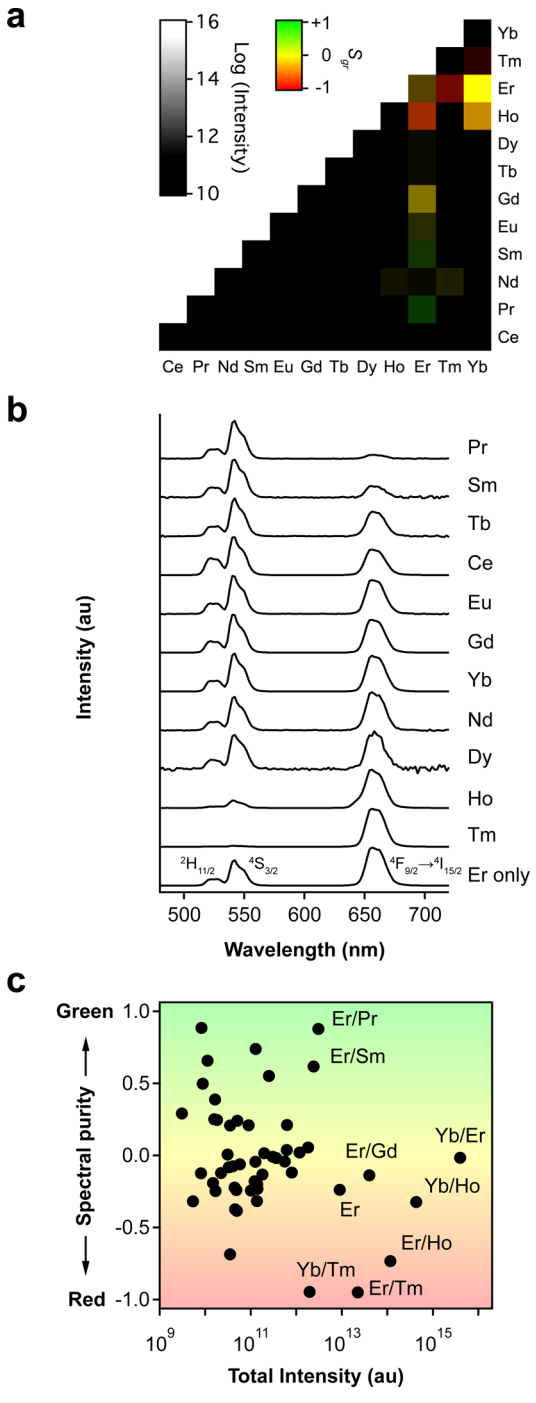


**Figure 1.** Combinatorial screening of doubly doped $NaYF_4$ nanocrystals. (a) Color map depicting the integrated UCL intensity and green/red spectral purity of 78 binary combinations of 12 lanthanide dopants (2/2 mol %) excited with $\lambda_{ex}$ = 980 nm at 10 W/cm$^2$. (b) Normalized upconverted luminescence spectra of $NaYF_4$ UCNPs with 2% $Er^{3+}$ and 1% codopant. (c) Green/red purity vs total intensity, integrated from 450 to 750 nm, for samples in part a, with estimated errors of ±0.05 and ±50%, respectively.

We quantified the green/red spectral purity, $S_{gr}$, of the nanoparticles' UCL using the equation

$$S_{gr} = \frac{A_g - A_r}{A_g + A_r} \quad (1)$$

where $A_g$ and $A_r$ are the integrated areas from 500 to 600 nm and from 600 to 700 nm, respectively. $S_{gr}$ values of +1 (−1) correspond to purely green (red) emission, while $S_{gr}$ = 0 indicates equal intensities of red and green emission.

$NaYF_4$ doped with $Er^{3+}/Tm^{3+}$ (2/2 mol %) exhibited almost completely pure red emission ($S_{gr}$ = −0.95, Figure 1c), while the $Er^{3+}/Ho^{3+}$ dopant pair exhibited somewhat less pure red emission ($S_{gr}$ = −0.73). Meanwhile, $NaYF_4$:$Er^{3+}/Pr^{3+}$ gave rise to highly pure green emission ($S_{gr}$ = +0.88) and $Er^{3+}/Sm^{3+}$ moderately pure ($S_{gr}$ = +0.61). The red-emitting pairs ($Er^{3+}/Tm^{3+}$ and $Er^{3+}/Ho^{3+}$) were an order of magnitude brighter than the green emitting pairs, although all of these "hits" from our initial screening were 2−3 orders of magnitude less intense than the highly optimized yet spectrally unselective, $Yb^{3+}$-sensitized UCNPs (Figure 1c). Considering that two-photon-excited fluorescence, the most common anti-Stokes technique for biological imaging, is over 5 orders of magnitude less intense than energy transfer upconversion in $Yb^{3+}/Er^{3+}$-doped materials,[8] we deemed the $Er^{3+}$-codoped combinations isolated in the initial screen to have sufficient intensity for imaging while providing the added advantage of spectral purity. Furthermore, additional optimization of spectrally pure probes, e.g., by adding an undoped shell,[7] will enhance the emission intensity.

**Correlating Dopant Concentrations with Spectral Purity.** Because energy transfer is dependent on the distance between donors and acceptors,[31] we reasoned that changing the $Er^{3+}$ and codopant concentrations might reveal spectrally pure emission for additional dopant combinations and would improve the spectral purity of emission from the dopant pairs identified in our initial screen. In a second library that varied the concentration of each codopant from 0 to 3% in the presence of 2% $Er^{3+}$, UCNPs codoped with $Tb^{3+}$, $Yb^{3+}$, $Dy^{3+}$, $Nd^{3+}$, $Eu^{3+}$, $Gd^{3+}$, or $Ce^{3+}$ still did not exhibit high green/red emission purity at any concentration (Figure 2a). For $Er^{3+}$ codoped with $Tm^{3+}$, $Ho^{3+}$, $Pr^{3+}$, or $Ho^{3+}$ (Figure 2a), we observed large enhancements in emission purity as the codopant concentration increased from 0 to 0.5%, with the purity saturating at 1% codopant. High codopant concentrations tended to reduce emission intensity, creating a point of


dx.doi.org/10.1021/nl3017994 | Nano Lett. XXXX, XXX, XXX−XXX

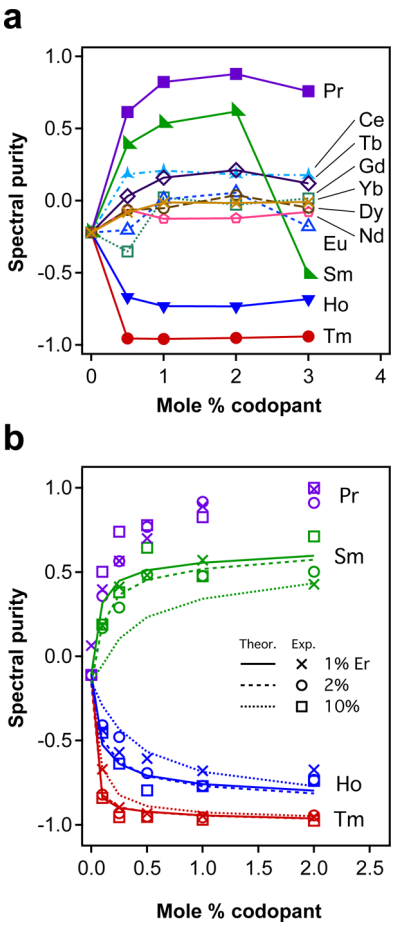


**Figure 2.** Spectral purity vs dopant concentration. (a) Green/red purity versus codopant concentration for $NaYF_4$:2% $Er^{3+}$ UCNPs codoped with 12 lanthanide ions. (b) Observed (symbols) and simulated (lines) green/red purity at three $Er^{3+}$ concentrations and five codopant concentrations for $NaYF_4$: $Er^{3+}$, $Ln^{3+}$ nanocrystals (Ln = Pr, Sm, Ho, Tm). $Er^{3+}/Pr^{3+}$ traces were not calculated due to praseodymium's known deviation from basic Judd–Ofelt theory.

co-optimized emission purity and intensity at approximately 0.5% codopant.

Using a third combinatorial assay to vary both the $Er^{3+}$ concentration and the codopant concentrations, we observed that the spectral purity was largely independent of $Er^{3+}$ concentration (Figure 2b). While $Er^{3+}$ concentrations greater than 2% in bulk materials tend to promote quenching via cross relaxation and energy migration,[32,33] increasing the $Er^{3+}$ concentration from 2 to 10% in our UCNPs increased the total emission intensity by five times without significantly reducing their spectral purity, lifetimes, or quantum yields. In fact, UCNPs doped with 10% $Er^{3+}$/ 0.5% $Tm^{3+}$ exhibited quantum yields of ~1% at 10 W/cm$^2$ excitation (Supporting Information, Table S12). Of central importance for biological imaging, the brightness of these spectrally pure probes is therefore maximal at high (10%) $Er^{3+}$ concentration and moderate (0.5%) codopant concentration.

**Theoretical Modeling and Validation.** Armed with a large experimental data set from our combinatorial libraries, we sought to develop and validate a theoretical model capable of rationalizing the realization of spectrally pure emission by codoping. The intensity of any given emission peak is proportional to the product of the population of the emitting state and the microscopic rate constant for the radiative transition. Hence, our model consists of a set of coupled differential equations describing the concentration $N_i$ of each lanthanide $4f^N$ manifold. We account for the population and depopulation of each manifold by electric dipole (ED) and magnetic dipole (MD) radiative transitions, nonradiative multiphonon relaxation (MPR), and energy transfer (ET), using eq 2:

$$\frac{dN_i}{dt} = \sum_j (N_j A_{ji}^{ED} - N_i A_{ij}^{ED}) + \sum_j (N_j A_{ji}^{MD} - N_i A_{ij}^{MD}) + (N_{i+1} W_{i+1,i}^{NR} - N_i W_{i,i-1}^{NR}) + \sum_{ij,kl} (N_j N_l P_{ji,lk}^{ET} - N_i N_k P_{ij,kl}^{ET}) \quad (2)$$

Here, $A_{ij}^{ED}$ and $A_{ij}^{MD}$ are the Einstein coefficients for ED and MD radiative transitions from manifold $i$ to $j$. $W_{i,i-1}^{NR}$ is the nonradiative MPR rate constant from manifold $i$ to the manifold immediately below $i$. $P_{ij,kl}^{ET}$ is the microscopic energy transfer parameter for the transfer of energy via the donor $i$ to $j$ transition and the acceptor $k$ to $l$ transition. The calculation of the thousands of rate constants represented in eq 2 is based on well-established theories and is described in more detail in the Supporting Information and elsewhere.[34] Briefly, ED transition rates are calculated using Judd–Ofelt theory,[35–37] while MD transition rates are calculated using the quantum mechanical magnetic dipole operator.[37] Nonradiative MPR is treated with a modified energy gap law,[38] and a related description of phonons is used to calculate phonon-assisted ET constants.[39] Finally, ET is considered to be assisted by energy migration[18,32] in the fast diffusion regime,[31] due to rapid and resonant donor–donor ET at the relatively high doping levels[32] considered in this study.

Combining the result of these calculations, we arrive at a computational model that generates rate constants for all possible transitions, numerically solves the simultaneous differential equations for the relevant manifolds (eq 2), and calculates emission spectra.

The theoretical spectral purity predicted by our kinetic model reproduces the experimental data with high fidelity (Figure 2b). While $Sm^{3+}$ conferred selectively green emission in the kinetic models, $Tm^{3+}$ and $Ho^{3+}$ conferred selectively red UCL, with $Tm^{3+}$ yielding more pure red emission than $Ho^{3+}$ for a given codopant concentration (Figure 2b). Just as in the experimental data, the theoretical results show that increasing the codopant concentration enhances the red or green spectral purity up to a saturation concentration (~0.5%), while increasing the $Er^{3+}$ concentration does not change the purity significantly. The minor discrepancies between theory and experiment can be attributed to the model's neglect of the surface contributions and the potential for inhomogeneous dopant distributions, particularly at the highest concentrations (10%).

The theoretical modeling also predicted radiative lifetimes and quantum yields (QY) that were comparable to observed values (Supporting Information, Table S12). For the red $^4F_{9/2} \rightarrow {}^4I_{15/2}$ transition of $NaYF_4$:$Er^{3+}$/$Tm^{3+}$ (10/0.5%) UCNPs, simulations predicted an average lifetime of 210 $\mu$s and a quantum yield of 0.85%, compared with observed values of 100 ± 20 $\mu$s and 1.3 ± 0.5% QY. Thus, our kinetic model is validated by experimental data acquired over a wide range of physical parameters, dopant combinations, and concentrations.


dx.doi.org/10.1021/nl3017994 | Nano Lett. XXXX, XXX, XXX–XXX

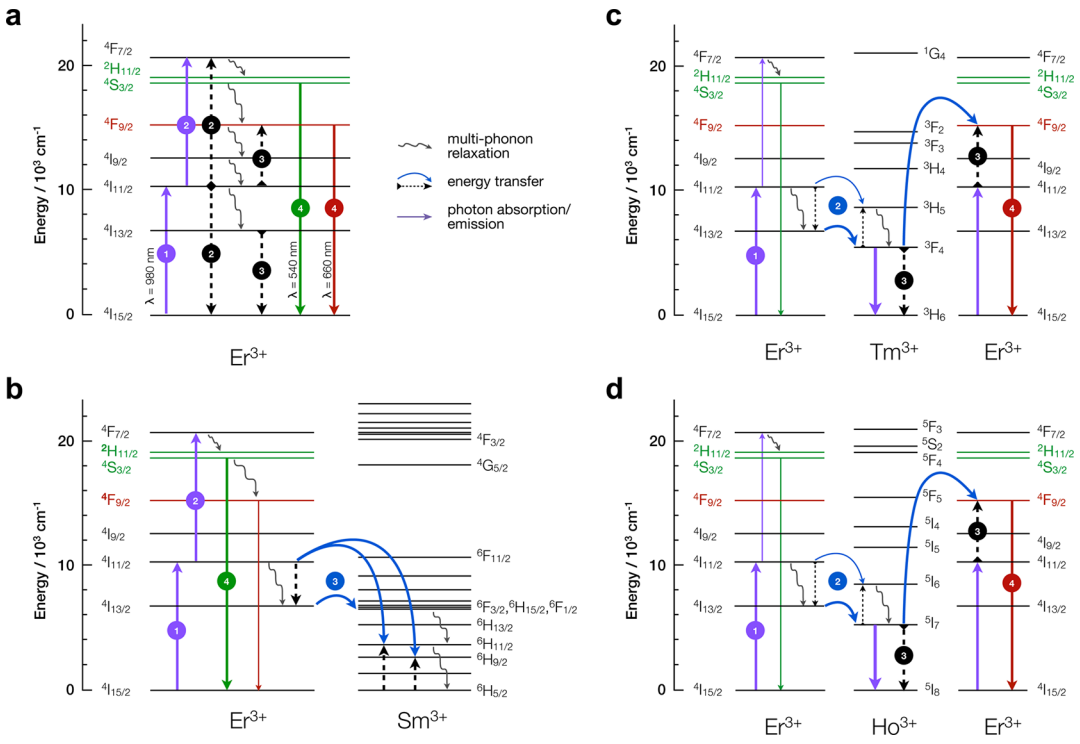


**Figure 3.** Energy transfer pathways for spectrally pure emission. Upconverted luminescence mechanisms for $NaYF_4$ nanocrystals doped with $Er^{3+}$ only (a), $Er^{3+}/Sm^{3+}$ (b), $Er^{3+}/Ho^{3+}$ (c), and $Er^{3+}/Tm^{3+}$ (d), at 2 mol % of each dopant. Arrows depict the transitions with the largest contributions to the population and depopulation of manifolds involved in visible emission, as calculated from kinetic models using $\lambda_{ex}$ = 980 nm at 10 W/cm$^2$. Modeling methodology, steady-state populations, and transition rates are detailed in the Supporting Information.

**Mechanisms Producing Spectrally Pure Emission.** To understand how $Tm^{3+}$, $Ho^{3+}$, $Pr^{3+}$, and $Sm^{3+}$ codopants induce spectrally pure emission from $Er^{3+}$, we examined the energy transfer pathways revealed by the validated kinetic model. As a reference, we first consider the upconversion mechanism in $NaYF_4$ UCNPs doped only with 2% $Er^{3+}$, which exhibit both green and red emission—a result of the comparable steady state populations and radiative rates of the $^4S_{3/2}$ and $^4F_{9/2}$ manifolds, respectively (Supporting Information, Tables S3 and S8). Here, the incident 980-nm radiation excites an $Er^{3+}$ ion in its $^4I_{15/2}$ ground state to the $^4I_{11/2}$ manifold (step 1, Figure 3a). A populated $^4I_{11/2}$ manifold can be excited again to the $^4F_{7/2}$ manifold via excited state absorption (ESA) of a second, 980-nm photon or via energy transfer upconversion (ETU) from a neighboring $Er^{3+}$ ion also excited to the $^4I_{11/2}$ manifold (step 2). The green-emitting $^2H_{11/2}$ and $^4S_{3/2}$ manifolds are then populated by sequential MPR from these high-energy $^4F_{7/2}$ manifolds. On the other hand, the red-emitting $^4F_{9/2}$ manifold is predominantly populated via ETU step 3, in which a $^4I_{13/2}\rightarrow{}^4I_{15/2}$ donor transition is coupled to a neighboring $^4I_{11/2}\rightarrow{}^4F_{9/2}$ transition. Thus, the ratio of green to red emission intensity is determined by the overall rate of the $^4F_{9/2}$-populating ETU step 3 relative to ETU/ESA Step 2, which preferentially populates $^2H_{11/2}$ and $^4S_{3/2}$.

The introduction of $Sm^{3+}$- to $Er^{3+}$-doped UCNPs results in preferentially green emission by quenching the intermediate states that take part in the critical ETU process—step 3 in Figure 3a—that populates the red-emitting $Er^{3+}(^4F_{9/2})$ manifold. Due to its high density of manifolds, $Sm^{3+}$ can accept energy over a large range of transition energies and can efficiently dissipate the energy via repeated MPR. $Sm^{3+}$ suppresses the $^4F_{9/2}$-populating ETU process by depopulating, via ET, the $Er^{3+}$ $^4I_{11/2}$ and $^4I_{13/2}$ manifolds by factors of 10 and 70, respectively (step 3, Figure 3b). Although $^4I_{11/2}$ is an important intermediate for generating both green and red emission, $^4I_{13/2}$ participates uniquely in the red emission process, meaning that the strong quenching of this state is the critical step in generating pure green emission in $Er^{3+}/Sm^{3+}$-doped UCNPs. This quenching mechanism is reminiscent of the proposed mechanism for $Ce^{3+}$-induced red emission from $Ho^{3+}$ articulated by Chen et al,[22] although direct quenching of the green-emitting manifold in $Ho^{3+}$ was also invoked in that case.

Conversely, the pure red emission that we found with $Er^{3+}/Tm^{3+}$-doped UCNPs is a result of *enhanced* and selective population of the red-emitting manifold, rather than selective quenching. The presence of $Tm^{3+}$ enhances the population of the red-emitting $Er^{3+}(^4F_{9/2})$ to 50 times that of the green emitting $Er^{3+}(^4S_{3/2})$ manifold. The electronic structure of $Tm^{3+}$ facilitates downhill energy transfer from the $Er^{3+}$ $^4I_{11/2}$ and $^4I_{13/2}$ manifolds to the $Tm^{3+}$ $^3H_5$ and $^3F_4$ manifolds, respectively (step 2, Figure 3c). However, unlike the $Sm^{3+}$ states populated by ET, there is a large energy gap between the $Tm^{3+}(^3F_4)$ manifold and the ground state (5800 cm$^{-1}$), essentially prohibiting relaxation via MPR. Hence, under 10 W/cm$^2$ excitation, the $^3F_4$ population reaches 7% of the total $Tm^{3+}$ concentration. The transferred energy is effectively stored in this $Tm^{3+}$ manifold and eventually promotes the population of the red-emitting $Er^{3+}(^4F_{9/2})$ manifold via ETU step 3 in Figure 3c. These efficient energy transfer pathways from the low-energy excited manifolds of $Er^{3+}$ ($^4I_{11/2}$, $^4I_{13/2}$) to the red-emitting state explain why cross-relaxation to those manifolds at high $Er^{3+}$ concentrations does not result in self-quenching when $Tm^{3+}$ is used a codopant. Thus, this mechanism for achieving


dx.doi.org/10.1021/nl3017994 | Nano Lett. XXXX, XXX, XXX−XXX

spectrally pure emission by selectively enhancing population in the emitting manifold is particularly powerful because of the potential to simultaneously achieve high UCL efficiency and high purity.

UCNPs doped with $Er^{3+}$ and $Ho^{3+}$ preferentially generate red emission by a mechanism analogous to that of $Er^{3+}/Tm^{3+}$, which is logical given the similar electronic structures of $Tm^{3+}$ and $Ho^{3+}$(Figure 3d). Energy is stored in the low-lying $Ho^{3+}(^5I_7)$ manifold, promoting ETU to the red-emitting $Er^{3+}(^4F_{9/2})$ manifold (step 3, Figure 3d). Detailed kinetic analysis shows that $Ho^{3+}$ is less efficient than $Tm^{3+}$ at promoting this red-enhancing energy transfer pathway because the rate of ETU step 3 is inversely proportional to the $2J+1$ multiplicity of the $Ho^{3+}(^5I_7)$ and $Tm^{3+}(^3F_4)$ states (Supporting Information, eq S2) and because the $Ho^{3+}(^5I_7)$ manifold has a lower energy than the $Tm^{3+}(^3F_4)$ manifold, leading to higher rates of back energy transfer (Supporting Information, Table S11). Thus, subtle differences in electronic structure can significantly alter spectral purity, necessitating broad combinatorial screening and thorough optimization of composition to realize probes with the highest spectral purity.

Generalizing from the mechanisms of $Er^{3+}/Tm^{3+}$- and $Er^{3+}/Ho^{3+}$-doped UCNPs, we suggest the following design rules for materials with efficient and spectrally pure upconverted luminescence:

1 The $4f^N$ manifold(s) that originate the desired radiative transitions should be populated via ETU from a low-energy, long-lived manifold.
2 The donor and acceptor transitions should have high oscillator strengths and should originate from highly populated manifolds so that the ET rate is comparable with radiative and multiphonon relaxation.
3 This critical ETU step should have a slightly downhill net energy to discourage back-transfer.

While the design rules above do not necessarily require multiple dopants, isolating a single dopant with an electronic structure that can fulfill all of the requirements would be unlikely and would restrict UCNPs to one emission color. Our comprehensive screening of two-dopant combinations showed that upconversion mechanisms hinging on two ETU steps offer more opportunity to favorably manipulate spectral purity than do the one-step mechanisms exemplified by $Yb^{3+}/Er^{3+}$ and $Er^{3+}/Sm^{3+}$.

**Triple Lanthanide Doping.** One limitation of $Er^{3+}/Tm^{3+}$-type mechanisms is that the low absorption cross section of $Er^{3+}$-codoped UCNPs at 980 nm cannot be decoupled from their high emission cross sections, since $Er^{3+}$ acts as both the absorbing and emitting ion. To overcome this restriction and discover a path to brighter, spectrally pure UCNP probes, we hypothesized that a third codopant could help decouple the absorption, emission, and energy transfer processes. Triple doping could result in combinations of properties found in binary-doped UCNPs, or it could reveal cooperative mechanisms not possible with only two dopants.

To map the far larger parameter space presented by triply doped UCNPs, we conducted a preliminary screen of the 220 combinations of $NaYF_4$ nanocrystals each doped with three lanthanide dopants, each at 2 mol %. As a spectrally agnostic purity parameter, we utilized the fourth standardized moment, $\beta_2$, of each emission spectrum:[40]

$$\beta_2 = \frac{\sum_\lambda I_\lambda(\lambda - \lambda)^4}{(\sum_\lambda I_\lambda(\lambda - \overline{\lambda})^2)^2} \quad (3)$$

Here, $I_\lambda$ is the area-normalized intensity at wavelength $\lambda$, and $\overline{\lambda}$ is the intensity-weighted mean wavelength. Since the kurtosis-related $\beta_2$ is a measure of the peakedness of a spectrum at $\overline{\lambda}$ and the length of its tails away from $\overline{\lambda}$, a spectrally pure emission spectrum that exhibits a single narrow peak has a large $\beta_2$, while spectra that exhibit no peaks or multiple peaks will have small $\beta_2$.[40]

The screening results (Figure 4a) indeed show that adding a third dopant can improve spectral purity, as with adding $Gd^{3+}$

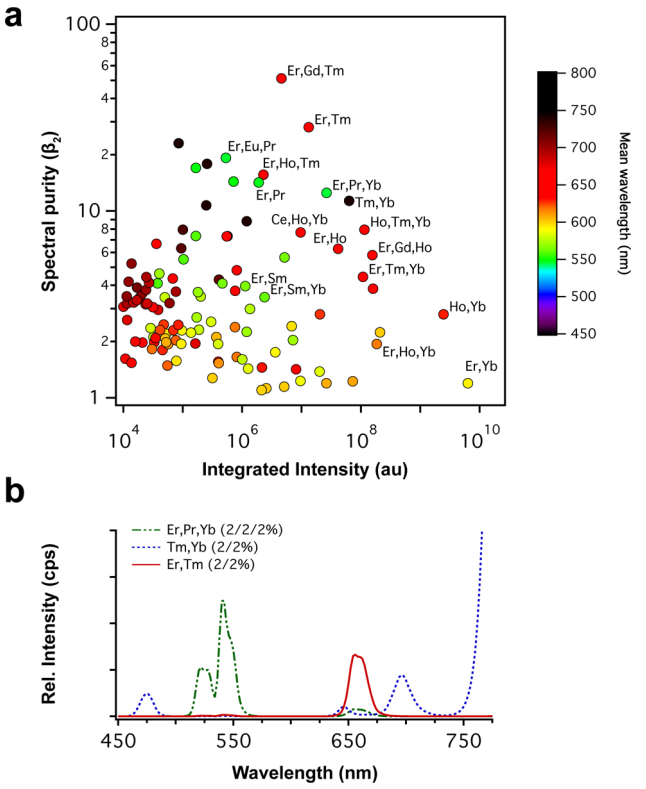


**Figure 4.** Optimizing spectral purity in triply doped UCNPs. (a) $\beta_2$ spectral purity vs intensity for $NaYF_4$ nanocrystals doped with three lanthanide ions each at 2 mol %. Color scale indicates the mean weighted wavelength of each point. Errors for selectivity and intensity are ±5% and ±50%, respectively. (b) UCL spectra for NaYF4 nanocrystals doped with $Er^{3+}/Pr^{3+}/Yb^{3+}$ (2/2/2%), $Ym^{3+}/Tb^{3+}$ (2/2%), and $Er^{3+}/Tm^{3+}$ (2/2%).

to $Er^{3+}/Tm^{3+}$-doped UCNPs, which yielded the most spectrally pure dopant combination. The addition of $Ce^{3+}$ or $Tm^{3+}$ codopants also conferred moderate red purity (654 nm) to bright-but-impure $Yb^{3+}/Ho^{3+}$-doped UCNPs, albeit with some reductions in intensity.

The addition of $Yb^{3+}$ increased the intensity of $Er^{3+}/Tm^{3+}$- and $Er^{3+}/Pr^{3+}$-doped UCNPs (Figure 4a), a result we ascribe to $Yb^{3+}$'s high absorption cross-section at 980 nm.[41] The addition of 2% $Yb^{3+}$ to $Er^{3+}/Pr^{3+}$-doped UCNPs increased the emission intensity by an order of magnitude without decreasing the $\beta_2$. In other words, the green emission purity is maintained. The addition of $Yb^{3+}$ to $Er^{3+}/Tm^{3+}$-, and $Er^{3+}/Ho^{3+}$-doped UCNPs, however, dramatically reduced their spectral purity. Hence, the addition of $Yb^{3+}$ as a sensitizer cannot be considered a universal strategy for enhancing the brightness of spectrally pure UCNPs.


dx.doi.org/10.1021/nl3017994 | Nano Lett. XXXX, XXX, XXX−XXX

Although elucidating the critical energy transfer pathways in these complex, triply doped UCNPs is challenging, we expect to gain further insight into controlling brightness and spectral purity by extending our computational methods in the future.

Ultimately, our combinatorial screening of doubly and triply doped $NaYF_4$ UCNPs revealed a set of three dopant combinations that emit bright and spectrally pure emission at three distinct visible wavelengths (Figure 4b). $Er^{3+}/Pr^{3+}/Yb^{3+}$-doped UCNP's emit at 540 nm with comparable purity and intensity to the 660 nm emission of $Er^{3+}/Tm^{3+}$, with all dopant concentrations at 2%. Meanwhile, UCNPs doped with $Yb^{3+}/Tm^{3+}$, well-known for their strong NIR UCL at 800 nm, can also be used as a third visible UC emitter at 475 or 700 nm. The minimal remaining overlap between the emission peaks of these three UCNP compositions can be easily deconvoluted so that true multiplexed imaging can be achieved with lanthanide-doped UCNP probes. There remains a broad, unutilized portion of the spectrum from 560 to 640 nm that invites the development of pure yellow- and orange-emitting probes that would enable simultaneous and prolonged five-color upconversion imaging.

**Conclusions.** We have demonstrated the synthesis and characterization of comprehensive libraries of upconverting $NaYF_4$ nanoparticles doped with two and three different lanthanide ions. We developed and validated a kinetic model that provided microscopic insight into the energy transfer pathways that result in spectrally pure emission in these multiply doped UCNPs. The near-zero spectral correlation and the narrow bandwidths of these "color-pure" emitters will enable the rapid and precise compositional analysis of heterogeneous biological samples without the need for complex deconvolution algorithms.

The combinatorial methods and kinetic models described here can be further exploited to explore additional material parameters in search of the ideal UCNPs for multicolor biological imaging. For instance, it is possible to screen the spectral purity and brightness of lanthanide dopant combinations excited at different NIR wavelengths,[41] encapsulated in various host matrices,[41] combined with transition metal dopants,[25,26,42] or embedded in a variety of doped heterostructures.[18,30,43] As the size of experimental space increases dramatically with the number of parameters, robust energy transfer models and data mining will be critical for predicting favorable materials, and high-throughput methods will be essential for validating candidate species. In this manner, a diversity of properties can be programmed into lanthanide-doped UCNPs by leveraging complex energy transfer pathways.

More generally, our combinatorial nanoparticle screening approach can be used as a primary method for tuning the composition of bulk materials for diverse optical applications.[44,45] Unlike the high-energy implantation of ions in thin films or the tedious grinding, melting, and polishing of solid-state synthetic methods, the solution-phase preparation of colloidal nanoparticles provides a straightforward mechanism for the combinatorial doping, processing, and screening of extensive libraries of materials. Ultimately, the systematic mapping and modeling of interactions between dopants will provide a valuable framework for the rational design of doped materials for any application requiring selectivity in optical or electronic transitions.

## ■ ASSOCIATED CONTENT

### Supporting Information

Experimental materials and methods, transmission electron micrographs, X-ray diffraction, kinetic theory, numerical methods, theoretical populations and transition rates, power dependence, quantum yields, and lifetime data. This information is available free of charge via the Internet at http://pubs.acs.org.

## ■ AUTHOR INFORMATION

### Corresponding Author

*E-mail: (E.M.C.) EMChan@lbl.gov; (D.J.M.) DMilliron@lbl.gov.

### Present Address

‡Department of Biochemistry and Molecular Pharmacology, University of Massachusetts, Medical School

### Notes

The authors declare no competing financial interest.

## ■ ACKNOWLEDGMENTS

The authors thank Jeffrey Urban, Brett Helms, and Omar Yaghi for helpful discussions. Rashid Zia and Christopher Dodson provided assistance with calculations. J.D.G. was supported by a SULI internship. D.J.M. was supported by a DOE Early Career Research Program award. This work was carried out entirely at the Molecular Foundry and was supported by the Office of Science, Office of Basic Energy Sciences, of the U.S. Department of Energy under Contract No. DE-AC02-05CH11231.

## ■ REFERENCES

(1) Vennerberg, D.; Lin, Z. *Sci. Adv. Mater.* **2011**, *3*, 26−40.
(2) Wang, F.; Liu, X. *Chem. Soc. Rev.* **2009**, *38*, 976−989.
(3) Wang, F.; Banerjee, D.; Liu, Y.; Chen, X.; Liu, X. *Analyst* **2010**, *135*, 1839−1854.
(4) Nam, S. H.; Bae, Y. M.; Park, Y. I.; Kim, J. H.; Kim, H. M.; Choi, J. S.; Lee, K. T.; Hyeon, T.; Suh, Y. D. *Angew. Chem., Int. Ed.* **2011**, *50*, 6093−6097.
(5) Wu, S.; Han, G.; Milliron, D. J.; Aloni, S.; Altoe, V.; Talapin, D. V.; Cohen, B. E.; Schuck, P. J. *Proc. Natl. Acad. Sci. U.S.A.* **2009**, *106*, 10917−10921.
(6) Zhang, F.; Haushalter, R. C.; Haushalter, R. W.; Shi, Y.; Zhang, Y.; Ding, K.; Zhao, D.; Stucky, G. D. *Small* **2011**, *7*, 1972−1976.
(7) Ostrowski, A. D.; Chan, E. M.; Gargas, D. J.; Katz, E. M.; Han, G.; Schuck, P. J.; Milliron, D. J.; Cohen, B. E. *ACS Nano* **2012**, *6*, 2686−2692.
(8) Auzel, F. *Chem. Rev.* **2004**, *104*, 139−173.
(9) Suijver, J. F. In *Luminescence: From Theory to Applications*; Ronda, C., Ed. Wiley-VCH: Weinheim, Germany, 2008; pp 133−178.
(10) Xiong, L.-Q.; Chen, Z.-G.; Yu, M.-X.; Li, F.-Y.; Liu, C.; Huang, C.-H. *Biomaterials* **2009**, *30*, 5592−5600.
(11) Carnall, W. T.; Goodman, G. L.; Rajnak, K.; Rana, R. S. *J. Chem. Phys.* **1989**, *90*, 3443−3457.
(12) Dejneka, M. J.; Streltsov, A.; Pal, S.; Frutos, A. G.; Powell, C. L.; Yost, K.; Yuen, P. K.; Müller, U.; Lahiri, J. *Proc. Natl. Acad. Sci. U.S.A.* **2003**, *100*, 389−393.
(13) Sohn, K.-S.; Park, D. H.; Cho, S. H.; Kim, B. I.; Woo, S. I. *J. Comb. Chem.* **2006**, *8*, 44−49.
(14) Maier, W. F.; Stoewe, K.; Sieg, S. *Angew. Chem., Int. Ed.* **2007**, *46*, 6016−6067.
(15) Cawse, J. N. *Acc. Chem. Res.* **2001**, *34*, 213−221.
(16) Wang, F.; Liu, X. *J. Am. Chem. Soc.* **2008**, *130*, 5642−5643.
(17) Wang, F.; Han, Y.; Lim, C. S.; Lu, Y.; Wang, J.; Xu, J.; Chen, H.; Zhang, C.; Hong, M.; Liu, X. *Nature* **2010**, *463*, 1061−1065.

(18) Wang, F.; Deng, R.; Wang, J.; Wang, Q.; Han, Y.; Zhu, H.; Chen, X.; Liu, X. *Nat. Mater.* **2011**, *10*, 968−973.
(19) Niu, W.; Wu, S.; Zhang, S. *J. Mater. Chem.* **2010**, *20*, 9113.
(20) Niu, W.; Wu, S.; Zhang, S.; Li, J.; Li, L. *Dalton Trans.* **2011**, *40*, 3305−3314.
(21) Mai, H.-X.; Zhang, Y.-W.; Sun, L.-D.; Yah, C.-H. *J. Phys. Chem. C* **2007**, *111*, 13721−13729.
(22) Chen, G.; Liu, H.; Somesfalean, G.; Liang, H.; Zhang, Z. *Nanotechnology* **2009**, *20*, 385704.
(23) Zou, X. L.; Shikida, A.; Yanagita, H.; Toratani, H. *J. Non-Cryst. Solids* **1995**, *181*, 100−109.
(24) Wang, G.; Peng, Q.; Li, Y. *Chem.—Eur. J.* **2010**, *16*, 4923−4931.
(25) Wang, J.; Wang, F.; Wang, C.; Liu, Z.; Liu, X. *Angew. Chem., Int. Ed.* **2011**, *50*, 10369−10372.
(26) Tian, G.; Gu, Z.; Zhou, L.; Yin, W.; Liu, X.; Yan, L.; Jin, S.; Ren, W.; Xing, G.; Li, S.; Zhao, Y. *Adv. Mater.* **2012**, *24*, 1226−1231.
(27) Ye, X.; Collins, J. E.; Kang, Y.; Chen, J.; Chen, D. T. N.; Yodh, A. G.; Murray, C. B. *Proc. Natl. Acad. Sci. U.S.A.* **2010**, *107*, 22430−22435.
(28) Chan, E. M.; Xu, C.; Mao, A. W.; Han, G.; Owen, J. S.; Cohen, B. E.; Milliron, D. J. *Nano Lett.* **2010**, *10*, 1874−1885.
(29) Roberts, J. E. *J. Am. Chem. Soc.* **1961**, *83*, 1087−1088.
(30) Mai, H.-X.; Zhang, Y.-W.; Sun, L.-D.; Yan, C.-R. *J. Phys. Chem. C* **2007**, *111*, 13730−13739.
(31) Thomas, D. D.; Carlsen, W. F.; Stryer, L. *Proc. Natl. Acad. Sci. U.S.A.* **1978**, *75*, 5746−5750.
(32) Snoeks, E.; Kik, P.; Polman, A. *Opt. Mater.* **1996**, *5*, 159−167.
(33) Zeng, J.; Su, J.; Li, Z.; Yan, R.; Li, Y. *Adv. Mater.* **2005**, *17*, 2119−2127.
(34) Chan, E. M.; Gargas, D. J.; Schuck, P. J.; Milliron, D. J. *J. Phys. Chem. B* **2012**, DOI: 10.1021/jp302401j.
(35) Judd, B. R. *Phys. Rev.* **1962**, *127*, 750−761.
(36) Ofelt, G. S. *J. Chem. Phys.* **1962**, *37*, 511−520.
(37) Walsh, B.; Barnes, N.; Di Bartolo, B. *J. Appl. Phys.* **1998**, *83*, 2772−2787.
(38) van Dijk, J. M. F.; Schuurmans, M. F. H. *J. Chem. Phys.* **1983**, *78*, 5317−5323.
(39) Miyakawa, T.; Dexter, D. *Phys. Rev. B* **1970**, *1*, 2961−2969.
(40) Balanda, K. P.; MacGillivray, H. L. *Am. Stat.* **1988**, *42*, 111−119.
(41) Takebe, H.; Murata, T.; Morinaga, K. *J. Am. Ceram. Soc.* **1996**, *79*, 681−687.
(42) Gamelin, D. R.; Güdel, H. U. *Acc. Chem. Res.* **2000**, *33*, 235−242.
(43) DiMaio, J. R.; Sabatier, C.; Kokuoz, B.; Ballato, J. *Proc. Natl. Acad. Sci. U.S.A.* **2008**, *105*, 1809−1813.
(44) Downing, E.; Hesselink, L.; Ralston, J.; Macfarlane, R. *Science* **1996**, *273*, 1185−1189.
(45) Grubb, S.; Bennett, K.; Cannon, R.; Humer, W. *Electron. Lett.* **1992**, *28*, 1243−1244.